12-4-2017

Ion parallel closures

Jeong-Young Ji
Utah State University, j.ji@usu.edu

Hankyu Q. Lee
Utah State University

Eric D. Held
Utah State University

Ion parallel closures

Journal-ref: Phys. Plasmas 24, 022127 (2017) with corrections

Jeong-Young Ji,[1,*] Hankyu Q. Lee,[1] and Eric D. Held[1]

[1]*Department of Physics, Utah State University, Logan, Utah 84322*

(Dated: December 4, 2017)

Abstract

Ion parallel closures are obtained for arbitrary atomic weights and charge numbers. For arbitrary collisionality, the heat flow and viscosity are expressed as kernel-weighted integrals of the temperature and flow-velocity gradients. Simple, fitted kernel functions are obtained from the 1600 parallel moment solution and the asymptotic behavior in the collisionless limit. The fitted kernel parameters are tabulated for various temperature ratios of ions to electrons. The closures can be used conveniently without solving the kinetic equation or higher order moment equations in closing ion fluid equations.

*Electronic address: j.ji@usu.edu

I. INTRODUCTION

The ion fluid equations for density (n), flow velocity $(\mathbf{V})$, and temperature (T) are closed by expressing heat flux density $(\mathbf{h})$ and viscosity tensor $(\boldsymbol{\pi})$ in terms of fluid variables, n, T, and $\mathbf{V}$. The ion friction force and collisional heating densities can be obtained from those of electrons [1]. For high collisionality, the ion closures are formulated in Ref. [2, 3] with the ion-electron collision effects ignored. The results are generalized and improved by including the ion-electron collision terms in Ref. [4]. For low collisionality the free streaming term plays an important role and the parallel closures appear in integral form [5–10]. With accurate collision terms adopted, the electron parallel closures for arbitrary collisionality are obtained in Refs. [11, 12].

The integral (non-local) closures enable fluid models to capture kinetic effects in parallel transport. The closures are implemented in the BOUT++ [13] to study kinetic effects on parallel transport in fluid models of the scrape-off layer [14, 15]. The kernel functions obtained from the moment approach may be approximated by a sum of modified-Helmholtz-equation solves in configuration space for the fast non-Fourier method to compute closures efficiently [16].

In this work we extend our previous work on parallel closures for electrons [11, 12] to ions. We adopt the closure/transport ordering ignoring the time derivative terms when solving general moment equations for higher order moments. As the ion-electron collision effects can be significant, we keep the ion-electron collision terms. The ion-electron collision operator notably modifies closures for high to moderate collisionality. The ion-electron collision terms depend on the ion-electron temperature ratio, $T_{\rm i}/T_{\rm e}$, and mass ratio combined with the ion charge number, $m_{\rm e}/m_{\rm i}Z^2 = m_{\rm e}/m_{\rm p}AZ^2$, where $m_{\rm e}$ is the electron mass, $m_{\rm i}$ is the ion mass, $m_{\rm p}$ is the proton mass, A is the atomic weight, and Z is the ion charge number. We solve the general moment equations for various temperature and mass ratios to obtain kernels to compute closures. Then we construct simple fitted kernels for arbitrary AZ^2 and temperature ratio $T_{\rm i}/T_{\rm e} \leq 10$. For $AZ^2 = 1$ and 2, the fitted kernels are specified by seven parameters, yielding highly accurate closures within 2% errors. For $AZ^2 \geq 3$, simpler form of kernels are specified by only four parameters which are expressed as general functions of AZ^2 and $T_{\rm i}/T_{\rm e}$, yielding accurate closures within 20% errors.

In Sec. II, we review the parallel moment equations and the properties of kernels for the integral closures. In Sec. III, the fitted kernels and their parameters are presented for arbitrary AZ^2. In Sec. IV, we summarize and discuss future work.

II. PARALLEL MOMENT EQUATIONS AND INTEGRAL CLOSURES

In this section we write a set of linearized parallel moment equations, the solution of which provides closures. The derivations are basically the same as the electron case in Sec. II of Ref. [12]. The parallel moment equations are obtained by taking parallel components of the general moment equations [17] or taking moments of the following reduced drift kinetic equation

$$v_\parallel \frac{\partial \bar{f}_{\rm i}^{\rm N}}{\partial \ell} = C_{\rm iL}(\bar{f}_{\rm i}^{\rm N}) - v_\parallel \frac{\partial \bar{f}_{\rm i}^{\rm M}}{\partial \ell} + C_{\rm iL}(\bar{f}_{\rm i}^{\rm M}) \tag{1}$$

where ℓ is the arc length along the magnetic field line, $\partial/\partial\ell = \mathbf{b}\cdot\nabla$, $\mathbf{b} = \mathbf{B}/B$, $\mathbf{B}$ is the magnetic field, and $\bar{f}^{\rm M}$ and $\bar{f}^{\rm N}$ are the gyro-averaged Maxwellian (M) and non-Maxwellian (N) distribution functions, respectively.

The linearized collision operators $C_{\rm iL}$ are linearized with respect to

$$f_a^{\rm m} = \frac{n_a}{\pi^{3/2} v_{Ta}^3} e^{-s_a^2},$$

where n_a is the density of species a, $v_{Ta} = \sqrt{2T_a/m_a}$, $s_a = v/v_{Ta}$, and T_a is the temperature. For the non-Maxwellian distribution,

$$C_{\rm iL}(\bar{f}_{\rm i}^{\rm N}) = C(\bar{f}_{\rm i}^{\rm N}, f_{\rm i}^{\rm m}) + C(f_{\rm i}^{\rm m}, \bar{f}_{\rm i}^{\rm N}) + C(\bar{f}_{\rm i}^{\rm N}, f_{\rm e}^{\rm m}) \tag{2}$$

and for the Maxwellian

$$C_{\rm iL}(\bar{f}_{\rm i}^{\rm M}) \approx C(f_{\rm i}^{\rm m}, f_{\rm e}^{\rm m}) + C(\bar{f}_{\rm i}^{\rm M-m}, f_{\rm e}^{\rm m}) + C(f_{\rm i}^{\rm m}, \bar{f}_{\rm e}^{\rm M-m}), \tag{3}$$

where

$$\bar{f}_a^{\rm M-m} \approx 2 s_{a\parallel} \frac{V_{a\parallel}}{v_{Ta}} f_a^{\rm m}$$

and $V_{a\parallel}$ is the parallel flow velocity. The ion-electron collision operator for the Maxwellian distribution, Eq. (3), which equilibrates temperature and flow velocity between electrons and ions, does not appear in the closure moment equations. Note that the ion-electron collision effect is not ignorable [4]. As explicitly shown in Eqs. (7), (9), and (12) of Ref. [4], the ion-electron collision operator depends on $\sqrt{m_{\rm e}/m_{\rm i}}/Z = \sqrt{m_{\rm e}/m_{\rm p} A Z^2}$ and the temperature ratio $T_{\rm e}/T_{\rm i}$.

The linearized parallel moment equations for the non-Maxwellian moments are [12]

$$\sum_{lk\neq {\rm M}} \psi^{jp,lk} \frac{\partial n^{lk}}{\partial \eta} = \sum_{lk\neq {\rm M}} c^{jp,lk} n^{lk} + g^{jp}, \tag{4}$$

or, in matrix form,

$$\Psi \frac{d}{d\eta}[n] = C[n] + [g], \tag{5}$$

where $d\eta = d\ell/\lambda_{\rm C}$, $\lambda_{\rm C} = v_{T{\rm i}}\tau_{\rm ii}$, and $\tau_{\rm ii}$ is the ion-ion collision time. Here and hereafter the ion species index will be suppressed unless it is needed for clarity. The matrix elements are

$$\begin{aligned} \psi^{jp,lk} &= \delta_{j+1,l}\psi^{j}_{pk} + \delta_{j-1,l}\psi^{j-1}_{kp}, \\ \psi^{j}_{pk} &= \frac{j+1}{\sqrt{(2j+1)(2j+3)}}(\sqrt{j+p+\tfrac{3}{2}}\delta_{p,k} - \sqrt{p}\delta_{p-1,k}), \end{aligned} \tag{6}$$

and

$$c^{jp,lk} = \delta_{jl}\tau_{\rm ii}(\hat{A}^{jpk}_{\rm ii} + \hat{B}^{jpk}_{\rm ii} + \hat{A}^{jpk}_{\rm ie}),$$

where $\hat{A}^{jpk}_{ab}$ and $\hat{B}^{jpk}_{ab}$ are explicitly formulated in Ref. [17]. The moment indices (l,k) run

$$\begin{gathered} (0,2),\ (0,3),\ \cdots,\ (0,K+1); \\ (1,1),\ (1,2),\ \cdots,\ (1,K); \\ (2,0),\ (2,1),\ \cdots,\ (2,K-1); \\ \vdots \quad \vdots \quad \vdots \\ (L,0),\ (L,1),\ \cdots,\ (L,K-1), \end{gathered}$$

excluding the Maxwellian moments ${\rm M} = (0,0),\ (0,1)$, and $(1,0)$.

The parallel closures are related to the general moments by

$$h_{\parallel} = -\frac{\sqrt{5}}{2} v_T T n^{11}, \tag{7}$$

$$\pi_{\parallel} = \frac{2}{\sqrt{3}} T n^{20}. \tag{8}$$

For ions, the only non-vanishing thermodynamic drives are

$$g^{11}_{\rm i} = \frac{\sqrt{5}}{2}\frac{n}{T}\frac{dT}{d\eta}, \tag{9}$$

$$g^{20}_{\rm i} = -\frac{\sqrt{3}}{2} n\tau_{\rm ii} W_{\parallel}, \tag{10}$$

where

$$W_{\parallel} = \mathbf{bb} : \mathsf{W},\ (\mathsf{W})_{\alpha\beta} = \partial_\alpha V_\beta + \partial_\beta V_\alpha - \frac{2}{3}\delta_{\alpha\beta}\nabla\cdot\mathbf{V} \tag{11}$$

and $\mathbf{V}$ is the ion flow velocity.

The system of N moment equations can be solved by computing the eigensystem of $\Psi^{-1}C$ where the eigenvalues appear in positive and negative pairs. Different from the electron case,

since the ion-electron collision matrix is not symmetric, some eigenvalues are complex numbers. The complex eigenvalues appear in complex conjugate pairs and so do the corresponding eigenvectors, making the solution real. The solution is expressed as a kernel weighted integral of the thermodynamic drives

$$n_A(z) = \sum_D \int_{-\infty}^{\infty} K_{AD}(z - z') g_D(z') dz', \tag{12}$$

where the moment indices have been abbreviated as a single index $A,\ B$, etc. The kernel functions are

$$K_{AD}(\eta) = \begin{cases} -\sum\limits_{\{B|\Re(k_B)>0\}}^{N} \gamma_{AD}^B e^{k_B \eta}, & \eta < 0, \\ +\sum\limits_{\{B|\Re(k_B)<0\}}^{N} \gamma_{AD}^B e^{k_B \eta}, & \eta > 0, \end{cases} \tag{13}$$

where $\Re(k_B)$ denotes the real part of the eigenvalue k_B. The coefficients are

$$\gamma_{AD}^B = \sum_C W_{AB} W_{BC}^{-1} \Psi_{CD}^{-1}, \tag{14}$$

where W_{AB} is the A-th component of the eigenvector with eigenvalue k_B.

For closure moments, we define

$$\begin{aligned} \gamma_{hh}^B &= \frac{5}{2} \gamma_{11,11}^B, \\ \gamma_{h\pi}^B &= -\sqrt{\frac{5}{3}} \gamma_{11,20}^B, \\ \gamma_{\pi h}^B &= -\sqrt{\frac{5}{3}} \gamma_{20,11}^B, \\ \gamma_{\pi\pi}^B &= \frac{4}{3} \gamma_{20,20}^B, \end{aligned} \tag{15}$$

and corresponding K_{AD} by Eq. (13). The sign should be corrected for $\gamma_{h\pi}^B$ and $\gamma_{R\pi}^B$ in Eq. (35) of Ref. 12. Noting that

$$\gamma_{AD}^{-B} = \begin{cases} -\gamma_{AD}^B, & AD = hh, \pi\pi \equiv \text{even}, \\ +\gamma_{AD}^B, & AD = h\pi, \pi h \equiv \text{odd}, \end{cases} \tag{16}$$

where $-B$ denotes the moment index corresponding to $-k_B$, we notice that the kernel functions are even or odd functions

$$K_{AD}(-\eta) = \begin{cases} +K_{AD}(\eta), & AD = \text{even} \\ -K_{AD}(\eta), & AD = \text{odd}. \end{cases} \tag{17}$$

Using the definition of K_{AD} and Eqs. (7-10), we can write the parallel closures

$$h_\parallel(\ell) \;=\; Tv_T \int d\eta' \Big(-\frac{1}{2}K_{hh}\frac{n}{T}\frac{dT}{d\eta'} - K_{h\pi}\frac{3}{4}n\tau W_\parallel\Big), \tag{18}$$

$$\pi_\parallel(\ell) \;=\; T \int d\eta' \Big(-K_{\pi h}\frac{n}{T}\frac{dT}{d\eta'} - K_{\pi\pi}\frac{3}{4}n\tau W_\parallel\Big). \tag{19}$$

For sinusoidal drives, $T = T_0 + T_1 \sin\varphi$ and $V_\parallel = V_0 + V_1 \sin\varphi$, where $\varphi = 2\pi\ell/\lambda + \varphi_0 = k\eta + \varphi_0$ and $k = 2\pi\lambda_{\rm C}/\lambda$, and assuming that n and $v_T \approx \sqrt{2T_0/m}$ are constant and $\nabla \cdot \mathbf{V}_\perp = 0$, the linearized closures become

$$h_\parallel(\ell) \;=\; -\frac{1}{2}nT_1 v_T \hat{h}_h \cos\varphi - nT_0 V_1 \hat{h}_\pi \sin\varphi, \tag{20}$$

$$\pi_\parallel(\ell) \;=\; -nT_1 \hat{\pi}_h \sin\varphi - nT_0 \frac{V_1}{v_T}\hat{\pi}_\pi \cos\varphi. \tag{21}$$

The dimensionless closures are defined by $\hat{h}_h = k\hat{K}_{hh}$, $\hat{h}_\pi = k\hat{K}_{h\pi}$, $\hat{\pi}_h = k\hat{K}_{\pi h}$, and $\hat{\pi}_\pi = k\hat{K}_{\pi\pi}$, where

$$\hat{K}_{AD} = \begin{cases} -\frac{1}{2}\sum_{B=1}^{N} \gamma_{AD}^B \left(\dfrac{1}{k_B + ik} + \dfrac{1}{k_B - ik}\right), & AD = \text{even} \\ \dfrac{i}{2}\sum_{B=1}^{N} \gamma_{AD}^B \left(\dfrac{1}{k_B + ik} - \dfrac{1}{k_B - ik}\right), & AD = \text{odd}, \end{cases} \tag{22}$$

which are derived from Eqs. (13), (16), and

$$\int K_{AD}(\eta - \eta')\cos(k\eta' + \varphi_0)d\eta' = \begin{cases} \hat{K}_{AD}\cos\varphi, & AD = \text{even}, \\ \hat{K}_{AD}\sin\varphi, & AD = \text{odd}. \end{cases} \tag{23}$$

Fig. 1 shows typical behavior of the kernels from $N = 100$ ($L = 10,\ K = 10$), $N = 400$ ($L = 20,\ K = 20$), and $N = 1600$ ($L = 40,\ K = 40$) moment calculations. With increasing number of moments, the kernels converge for smaller η. However, convergence is slow. For $\eta \ll 1$, analytical calculations show that the kernels approach [18]

$$K_{hh}(\eta) \;\approx\; -\frac{18}{5\pi^{3/2}}(\ln|\eta| + \gamma_h), \tag{24}$$

$$K_{h\pi}(\eta) \;\approx\; \frac{1}{5}, \tag{25}$$

$$K_{\pi h}(\eta) \;\approx\; \frac{1}{5}, \tag{26}$$

$$K_{\pi\pi}(\eta) \;\approx\; -\frac{4}{5\pi^{1/2}}(\ln|\eta| + \gamma_\pi), \tag{27}$$

where γ_h and γ_π are constants. Fig. 2 shows the corresponding closures. The $N = 1600$ moment closures converge for $k \lesssim 100$ and reach collisionless values at $k \sim 30$. This situation is very

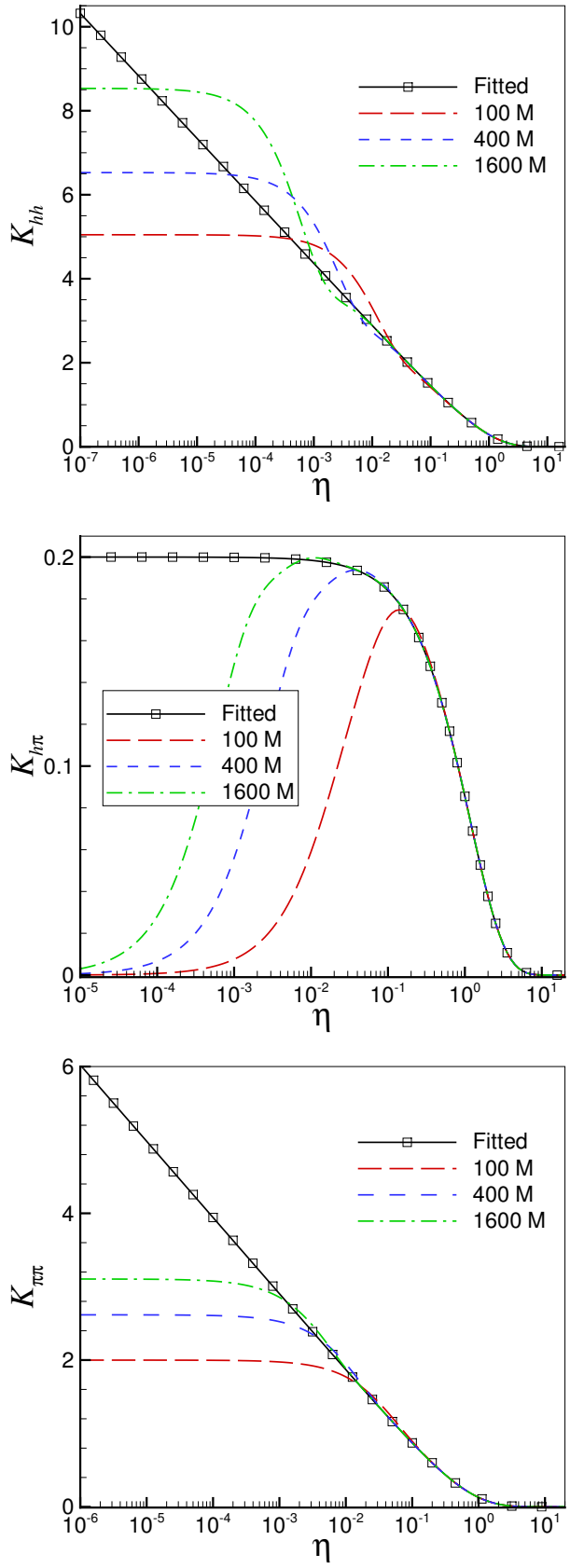

Figure 1: Kernels for $AZ^2 = 1$ and $T_\mathrm{i}/T_\mathrm{e} = 4$. The kernel $K_{\pi h}$ (not shown) is similar to $K_{h\pi}$.

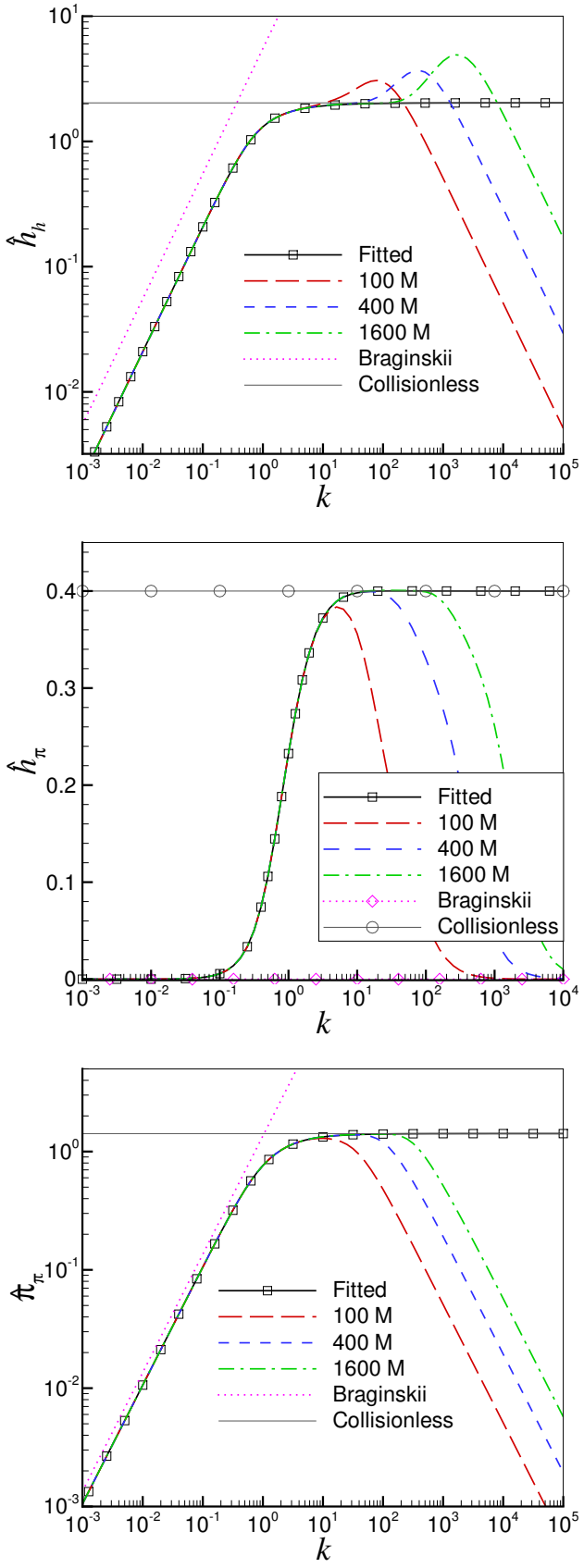

Figure 2: Closures for $AZ^2 = 1$ and $T_\mathrm{i}/T_\mathrm{e} = 4$. The closure $\hat{\pi}_h$ (not shown) is similar to $\hat{h}_\pi$.

different from the electron case where even the $N = 6400$ moment closures do not reach the collisionless values in the convergent regime $k \lesssim 100$ (see Fig. 2 of Ref. [11]). The convergence of the electron closures is slower than the ion closures. This is because the coupling between moments of different velocity orders in the electron-ion collision operator is much larger than that in the ion-electron operator. Deviations of moment closures for large $k \gtrsim 100$ will be amended by collisionless kernels for small η. Finally the corrections to Braginskii provided by the moment closures, $\hat{h}_h$ and $\hat{\pi}_\pi$, even in the highly collisional regime are due to the inclusion of the ion-electron collision operator.

III. FITTED KERNELS FOR INTEGRAL CLOSURES

As shown in Figs. 1 and 2, the kernels obtained from a finite number of moment equations are not accurate for small η and result in inaccurate closures in the collisionless limit. Furthermore they involve as many terms as the number of moments used in the derivation [see Eq. (13)]. Therefore simple fitted functions are desirable to accurately represent the moment kernels for the convergent regime and the collisionless kernels for small η. Due to the ion-electron collision operator in Eq. (2), the kernels depend on AZ^2 and $T_\mathrm{i}/T_\mathrm{e}$. By computing the kernels and closures for $AZ^2 = 1, 2, 3, 4, 16, \cdots, 4096$ and $T_\mathrm{i}/T_\mathrm{e} = 0,\ 0.01,\ 0, 1,\ 1,\ 2, \cdots,\ 10$, highly accurate fitted kernels for arbitrary AZ^2 and $T_\mathrm{i}/T_\mathrm{e} \lesssim 10$ may be obtained via interpolation.

A. Kernels for $AZ^2 = 1\,(\mathrm{H}^+)$ and $2\,(\mathrm{D}^+)$

As in the electron case, all kernel functions can be fitted to a single function

$$K_{AB}(\eta) = -[d + a\exp(-b\eta^c)]\ln[1 - \alpha\exp(-\beta\eta^\gamma)] \tag{28}$$

which yields highly accurate closures for arbitrary collisionality. In order to reproduce the collisionless-limit kernels (24-27), the parameter a is derived from other parameters

$$a = \frac{18}{5\pi^{3/2}\gamma} - d \text{ for } K_{hh}, \tag{29}$$

$$a = \frac{4}{5\pi^{1/2}\gamma} - d \text{ for } K_{\pi\pi}, \tag{30}$$

and

$$a = -d - \frac{1}{5\ln(1-\alpha)} \text{ for } K_{h\pi} \text{ and } K_{h\pi}. \tag{31}$$

	a	b	c	d	α	β	γ	err.
K_{hh}	0.141	1.86	0.721	0.974	1	0.823	0.58	0.2%
$K_{\pi h}$	-0.750	1.23	0.600	1.10	0.434	1.28	0.502	1.6%
$K_{h\pi}$	-0.701	1.30	0.602	1.07	0.42	1.24	0.510	0.6%
$K_{\pi\pi}$	0.440	0.641	0.791	0.319	1	1.09	0.595	0.3%

Table I: Fitted parameters in Eq. (28) with no ion-electron collision operator (in the $AZ^2 \to \infty$ and/or $T_\mathrm{i}/T_\mathrm{e} \to 0$ limits).

In the collisional limit, the kernels also reproduce Braginskii-type parallel closures [4]

$$h_\parallel = -\hat{\kappa}_\parallel \frac{nT\tau_\mathrm{ii}}{m}\partial_\parallel T, \tag{32}$$

$$\pi_\parallel = -\hat{\eta}_0 nT\tau_\mathrm{ii} W_\parallel \tag{33}$$

with improved coefficients by including ion-electron collision effects and more moments.

In the $AZ^2 \to \infty$ and/or $T_\mathrm{i}/T_\mathrm{e} \to 0$ limits, the ion-electron collision terms vanish and the fitted parameters are presented in Table I. In the collisional limit, the closure coefficients become Braginskii's coefficients $\hat{\kappa}_\parallel = \int_{-\infty}^{\infty} K_{hh} d\eta \approx 5.586$ and $\hat{\eta}_0 = \int_{-\infty}^{\infty} \frac{3}{4} K_{\pi\pi} d\eta \approx 1.365$ where the values are slightly improved from Braginskii's due to the increased number of moments.

As $T_\mathrm{i}/T_\mathrm{e}$ increases, ion-electron collisions become significant. The effect is more significant for smaller values of AZ^2 due to the factor $1/\sqrt{AZ^2}$ in the ion-electron collision terms. The fitted parameters for $AZ^2 = 1\,(\mathrm{H}^+)$ and $2\,(\mathrm{D}^+)$ are presented in Tables II and III, respectively. The fitted kernels for $AZ^2 = 1$ and $T_\mathrm{i}/T_\mathrm{e} = 4$ are shown in Fig. 1 and the corresponding closures are shown in Fig. 2. Note that computed closures approach collisional and collisionless closures in the $k \to 0$ and ∞ limits, respectively.

To evaluate the accuracy of fitted kernels, closures computed from the fitted kernels are compared with 1600 moment closures computed from Eq. (22) in the convergent regime $k \lesssim 80$. Maximum percentage errors are at most 1.9% at a specific temperature ratio and less than 1% at most temperature ratios as shown in Tables II and III. For a temperature ratio $t = T_\mathrm{i}/T_\mathrm{e}$, not listed in the Tables II and III, parameters can be obtained from a simple linear interpolation between two temperature ratios t_1 and t_2 ($t_1 < t < t_2$)

$$\Gamma(t) = \frac{t_2 - t}{t_2 - t_1}\Gamma(t_1) + \frac{t - t_1}{t_2 - t_1}\Gamma(t_2) \tag{34}$$

K_{AB}	$T_\mathrm{i}/T_\mathrm{e}$	0.01	0.1	1	2	3	4	5	6	7	8	9	10
K_{hh}	a	0.161	0.190	0.130	0.0723	0.0353	0.0116	-0.00597	-0.0179	-0.0209	0.000474	0.0145	0.0234
	b	1.77	1.77	1.77	1.79	1.81	1.82	1.82	1.82	1.82	1.74	1.59	1.51
	c	0.660	0.646	0.630	0.610	0.581	0.554	0.537	0.519	0.5	0.461	0.416	0.363
	d	0.954	0.942	0.930	0.850	0.780	0.719	0.669	0.625	0.579	0.500	0.435	0.375
	α	1	1	1	1	1	1	1	1	1	1	1	1
	β	0.811	0.814	0.857	0.907	0.993	1.11	1.27	1.47	1.71	1.96	2.30	2.81
	γ	0.579	0.570	0.61	0.701	0.793	0.885	0.975	1.07	1.16	1.29	1.44	1.62
	err.	0.6%	1.0%	0.5%	0.7%	0.6%	0.6%	0.5%	0.7%	0.5%	0.6%	0.6%	0.6%
$K_{\pi h}$	a	-0.750	-0.678	-0.405	-0.146	-0.0296	0.0295	0.0650	0.119	0.160	0.218	0.280	0.331
	b	1.23	1.45	1.45	1.56	1.68	1.78	1.94	1.95	1.96	1.96	1.95	1.96
	c	0.600	0.616	0.624	0.671	0.780	0.830	0.899	0.923	0.946	0.981	1.02	1.03
	d	1.10	1.04	0.766	0.521	0.448	0.419	0.418	0.398	0.356	0.315	0.252	0.243
	α	0.435	0.426	0.425	0.413	0.380	0.36	0.339	0.321	0.321	0.313	0.313	0.295
	β	1.28	1.25	1.05	0.791	0.683	0.677	0.736	0.775	0.839	0.903	0.952	1.13
	γ	0.502	0.501	0.585	0.765	0.943	1.08	1.19	1.33	1.46	1.61	1.79	1.88
	err.	1.5%	1.9%	1.0%	0.5%	0.6%	0.5%	0.6%	0.3%	0.3%	0.3%	0.3%	0.5%
$K_{h\pi}$	a	-1.06	-1.19	-0.789	-0.354	-0.0270	0.221	0.574	1.16	1.57	1.70	1.21	0.951
	b	1.37	1.41	1.58	1.72	1.93	2.03	2.11	2.12	2.13	2.70	3.10	3.53
	c	0.604	0.611	0.619	0.644	0.693	0.723	0.739	0.774	0.793	0.817	0.818	0.819
	d	1.73	1.87	1.72	1.47	1.18	1.06	0.829	0.338	-0.0193	-0.0321	-0.0478	-0.0543
	α	0.257	0.254	0.194	0.164	0.159	0.145	0.133	0.125	0.121	0.113	0.158	0.2
	β	1.24	1.29	1.06	0.937	0.934	1.03	1.09	0.827	0.326	0.331	0.513	0.76
	γ	0.504	0.490	0.584	0.725	0.857	0.965	1.12	1.59	1.62	1.86	2.07	1.97
	err.	1.4%	1.5%	0.3%	0.4%	0.3%	0.7%	0.5%	0.8%	1.3%	1.3%	1.0%	1.1%
$K_{\pi\pi}$	a	0.448	0.439	0.392	0.248	0.133	0.0801	0.0398	0.0193	6.00×10^{-5}	-0.0154	-0.0359	-0.0512
	b	0.642	0.657	0.657	0.738	0.966	1.11	1.42	1.48	1.55	1.66	1.70	1.81
	c	0.788	0.788	0.810	0.882	0.972	1.01	1.05	1.12	1.14	1.15	1.26	1.28
	d	0.316	0.324	0.340	0.407	0.461	0.469	0.474	0.468	0.463	0.458	0.459	0.458
	α	1	1	1	1	1	1	1	1	1	1	1	1
	β	1.09	1.09	1.134	1.22	1.34	1.48	1.65	1.84	2.06	2.32	2.63	2.97
	γ	0.591	0.591	0.617	0.689	0.761	0.822	0.878	0.927	0.975	1.02	1.07	1.11
	err.	0.5%	0.4%	0.6%	0.4%	0.4%	0.3%	0.4%	0.3%	0.3%	0.2%	0.3%	0.2%

Table II: Fitted parameters in Eq. (28) for $AZ^2 = 1$.

for $\Gamma = b, c, d, \alpha, \beta, \gamma$. The parameter a can be obtained from the interpolated values by using Eqs. (29), (30) and (31). The closures computed from the interpolated parameters show similar accuracy. For $T_\mathrm{i}/T_\mathrm{e} < 0.01$, the ion-electron collision effect is ignorable and the parameters of Table I produce accurate closures within 2% error.

K_{AB}	$T_\mathrm{i}/T_\mathrm{e}$	0.01	0.1	1	2	3	4	5	6	7	8	9	10
K_{hh}	a	0.144	0.159	0.113	0.0634	0.0316	0.00509	-0.0217	-0.0422	-0.0540	-0.0845	-0.121	-1.24
	b	1.94	2.20	2.42	2.7	2.91	1.72	1.23	0.9	0.843	0.597	0.434	0.393
	c	0.720	0.735	0.749	0.77	0.8	1.00	1.47	1.47	1.40	1.29	1.25	1.2
	d	0.973	0.969	0.955	0.898	0.837	0.788	0.736	0.691	0.650	0.633	0.630	0.6
	α	1	1	1	1	1	1	1	1	1	1	1	1
	β	0.821	0.823	0.846	0.887	0.946	1.03	1.12	1.22	1.36	1.53	1.75	2.01
	γ	0.579	0.573	0.606	0.672	0.744	0.815	0.905	0.996	1.09	1.18	1.27	1.36
	err.	0.2%	0.9%	0.4%	0.6%	0.6%	0.7%	0.4%	0.4%	0.3%	0.3%	0.3%	0.4%
$K_{\pi h}$	a	-0.750	-0.688	-0.431	-0.169	-0.0524	-0.00959	0.0170	0.0454	0.0659	0.108	0.153	0.206
	b	1.23	1.40	1.43	1.62	1.7	1.83	1.84	1.86	1.85	1.85	1.85	1.86
	c	0.600	0.608	0.619	0.670	0.673	0.673	0.777	0.880	0.895	0.955	0.990	1.02
	d	1.10	1.07	0.789	0.514	0.367	0.303	0.274	0.243	0.222	0.208	0.209	0.204
	α	0.434	0.409	0.428	0.44	0.47	0.494	0.497	0.500	0.500	0.470	0.424	0.386
	β	1.28	1.24	1.06	0.807	0.661	0.620	0.618	0.615	0.641	0.646	0.698	0.749
	γ	0.502	0.504	0.573	0.722	0.882	1.01	1.13	1.26	1.37	1.52	1.64	1.77
	err.	1.5%	1.2%	1.5%	0.5%	0.4%	0.3%	0.2%	0.2%	0.6%	0.5%	0.3%	0.3%
$K_{h\pi}$	a	-1.06	-1.13	-0.577	-0.273	-0.119	0.0440	0.229	0.363	0.521	0.686	0.638	0.440
	b	1.37	1.42	1.69	1.84	1.84	1.84	1.84	1.97	2.18	2.40	2.41	2.71
	c	0.599	0.613	0.630	0.659	0.691	0.750	0.749	0.758	0.797	0.844	0.823	0.817
	d	1.75	1.82	1.27	0.975	0.821	0.658	0.473	0.338	0.182	0.0534	-0.00799	-0.0116
	α	0.253	0.254	0.251	0.248	0.248	0.248	0.248	0.248	0.248	0.237	0.272	0.373
	β	1.23	1.27	1.03	0.900	0.895	0.892	0.853	0.853	0.704	0.35	0.209	0.276
	γ	0.509	0.496	0.580	0.699	0.799	0.915	1.07	1.24	1.60	2.61	2.18	2.26
	err.	0.8%	1.7%	0.5%	0.7%	0.6%	0.2%	0.5%	0.4%	0.6%	0.8%	1.2%	0.6%
$K_{\pi\pi}$	a	0.446	0.441	0.405	0.294	0.186	0.106	0.0558	0.0255	0.0139	-0.0116	-0.0284	-0.0661
	b	0.641	0.652	0.652	0.692	0.816	1.07	1.54	2.64	1.22	1.10	1.07	1.04
	c	0.789	0.789	0.805	0.856	0.923	1.00	1.10	1.26	1.79	1.89	1.67	1.67
	d	0.317	0.321	0.334	0.384	0.436	0.471	0.486	0.488	0.478	0.480	0.478	0.495
	α	1	1	1	1	1	1	1	1	1	1	1	1
	β	1.09	1.09	1.12	1.19	1.27	1.37	1.48	1.62	1.77	1.94	2.12	2.35
	γ	0.592	0.592	0.611	0.666	0.725	0.782	0.833	0.879	0.918	0.965	1.00	1.05
	err.	0.6%	0.3%	0.3%	0.9%	0.5%	0.4%	0.4%	0.4%	0.7%	0.4%	0.3%	0.3%

Table III: Fitted parameters in Eq. (28) for $AZ^2 = 2$.

B. Kernels for $AZ^2 \geq 3$

One can continue with Eq. (28) to obtain fitted parameters which are accurate to within 2% error for arbitrary $AZ^2 \geq 3$. When AZ^2 is large, however, the ion-electron collision effect becomes less significant and a simpler fitted function may suffice to represent the moment kernels with

K_{AB}	Γ	a_{00}	a_{11}	a_{12}	a_{13}	a_{21}	a_{22}	a_{23}	a_{31}	a_{32}	a_{33}
K_{hh}	α	1	0	0	0	0	0	0	0	0	0
	β	0.879	0.524	-0.144	0.01	-1.87	0.533	-0.0335	1.96	-0.545	0.035
	γ	0.58	-0.213	0.1	-0.00613	0.824	-0.256	0.0152	-0.846	0.245	-0.0142
$K_{\pi h}$	α	0.862	-0.0022	0.0009	0.0013	0.442	-0.015	-0.0267	-0.529	-0.17	0.0572
	β	0.235	0.344	-0.0925	0.0065	-1.67	0.471	-0.021	1.88	-0.432	0.0103
	γ	1.02	-0.252	0.128	-0.0089	1.92	-0.674	0.0404	-2.43	0.747	-0.04
$K_{h\pi}$	α	0.862	-0.0242	0.0447	-0.0071	0.665	-0.417	0.024	-0.613	0.123	0.0197
	β	0.235	0.339	-0.1	0.011	-1.88	0.785	-0.058	2.09	-0.765	0.0505
	γ	1.02	-0.156	0.104	-0.0107	1.27	-0.737	0.0671	-1.5	0.832	-0.0731
$K_{\pi\pi}$	α	1	0	0	0	0	0	0	0	0	0
	β	1.18	0.0688	0.0052	-0.0001	0.107	-0.0393	0.0035	-0.27	0.087	-0.0063
	γ	0.705	-0.0044	0.021	-0.0011	0.0288	-0.0239	0.0005	-0.0334	0.0192	-0.0003

Table IV: Coefficients in Eq. (36) for the fitted parameters in Eq. (35).

collisionless asymptotes. For $AZ^2 \geq 3$, we adopt the following form for the fitted kernels

$$K_{AB}(\eta) = -\kappa \ln[1 - \alpha \exp(-\beta \eta^\gamma)]. \tag{35}$$

Using the parameters α, β, and γ obtained for $AZ^2 = 3,\ 16,\ 64$ and for $T_{\rm i}/T_{\rm e} = 0,\ 1,\ 5,\ 9$, the following interpolation formula is obtained for $\Gamma = \alpha, \beta, \gamma$

$$\Gamma(t,x) = (a_{33}t^2 + a_{32}t + a_{31})tx^3 + (a_{23}t^2 + a_{22}t + a_{21})tx^2 + (a_{13}t^2 + a_{12}t + a_{11})tx + a_{00} \tag{36}$$

where $t = T_{\rm i}/T_{\rm e}$ and $x = 1/\sqrt{AZ^2}$. The coefficients a_{ij} for $AB = hh,\ h\pi,\ \pi h$, and $\pi\pi$ are presented in Table IV. The parameter κ can be obtained from the collisionless constraints (24-27),

$$\kappa = \begin{cases} \dfrac{18}{5\pi^{3/2}\gamma}, & \text{for } K_{hh} \\ \dfrac{4}{5\pi^{1/2}\gamma}, & \text{for } K_{\pi\pi} \\ -\dfrac{1}{5\ln(1-\alpha)}, & \text{for } K_{h\pi} \text{ and } K_{\pi h} \end{cases} . \tag{37}$$

The simple fitted kernel (35) with the coefficients (36) is tested for $AZ^2 = 3,\ 4,\ 8,\ 12,\ 16,\ 32,\ 64,\ 256,\ 1024,\ 4096$ and $T_{\rm i}/T_{\rm e} = 10^{-4},\ 10^{-3},\ 10^{-2},\ 10^{-1},\ 1,\ 2,\ 3,\ \cdots,\ 10$. The kernel yields accurate closures within 5% errors for $\hat{h}_h$ and $\hat{\pi}_\pi$ and within 20% errors for $\hat{h}_\pi$ and $\hat{\pi}_h$. The errors greater than 10% for $\hat{h}_\pi$ and $\hat{\pi}_h$ occur at small closure values only. Since the major contribution to closures are from the diagonal elements $\hat{h}_h$ and $\hat{\pi}_\pi$, the total closures computed from the fitted kernels (35) are expected to be accurate to within 10% error in most cases.

IV. SUMMARY AND FUTURE WORK

For ion parallel closures, the heat flow and viscosity closures are expressed by kernel weighted integrals of temperature and flow velocity gradients. Simple fitted kernels are obtained by solving the linearized parallel moment equations for arbitrary atomic weights and charge numbers. This work together with previous work on electrons [12] completes parallel closures for fully ionized electron-ion plasmas for cases where the magnetic field strength does not vary significantly along the field line.

The moment method can be applied to the Landau fluid closures in Ref. [19] to obtain the exact linear response for arbitrary collisionality. In the Landau fluid models, the parallel moments are decomposed into parallel and perpendicular parts. Therefore the Landau fluid closures can be constructed as linear combination of parallel moments with higher order moments included. The Landau fluid closures for the $3_{\parallel} + 1_{\perp}$ model obtained from the moment method will be presented in the near future.

While the linearized moment equations allow analytical expressions of the linear response theory, they do not capture coupling effects between temperature and magnetic field gradients and the moments. The linear response theory should be a good approximation whenever the variations in the temperature and magnetic field along a field line are small. For large variations of temperature and magnetic field, efforts to include coupling effects of magnetic-field inhomogeneity and temperature variations are ongoing.

Acknowledgments

The research was supported by the U.S. DOE under grant nos. DE-SC0014033, DE-SC0016256, DE-FC02-08ER54973, and DE-FG02-04ER54746, and by the project PE15090 of Korea Polar Research Institute. This work was performed in conjunction with the Plasma Science and Innovation (PSI) center and the Center for Extended MHD Modeling (CEMM).

---

[1] J.-Y. Ji and E. D. Held, Phys. Plasmas **20**, 042114 (2013).

[2] S. I. Braginskii, Sov. Phys. JETP **6**, 358 (1958).

[3] S. I. Braginskii, in *Reviews of Plasma Physics*, edited by M. A. Leontovich (Consultants Bureau, New York, 1965), vol. 1, p. 205.

[4] J.-Y. Ji and E. D. Held, Phys. Plasmas **22**, 062114 (2015).

[5] G. W. Hammett and F. W. Perkins, Phys. Rev. Lett. **64**, 3019 (1990).

[6] R. D. Hazeltine, Phys. Plasmas **5**, 3282 (1998).

[7] E. D. Held, J. D. Callen, C. C. Hegna, and C. R. Sovinec, Phys. Plasmas **8**, 1171 (2001).

[8] E. D. Held, Phys. Plasmas **10**, 4708 (2003).

[9] E. D. Held, J. D. Callen, and C. C. Hegna, Phys. Plasmas **10**, 3933 (2003).

[10] E. D. Held, J. D. Callen, C. C. Hegna, C. R. Sovinec, T. A. Gianakon, and S. E. Kruger, Phys. Plasmas **11**, 2419 (2004).

[11] J.-Y. Ji and E. D. Held, Phys. Plasmas **21**, 122116 (2014).

[12] J.-Y. Ji, S.-K. Kim, E. D. Held, and Y.-S. Na, Phys. Plasmas **23**, 032124 (2016).

[13] B. D. Dudson, M. V. Umansky, X. Q. Xu, P. B. Snyder, and H. R. Wilson, Comput. Phys. Comm. **180**, 1467 (2009).

[14] J. T. Omotani and B. D. Dudson, Plasma Phys. Control. Fusion **55**, 055009 (2013).

[15] J. T. Omotani, B. D. Dudson, E. Havlíčková, and M. Umansky, J. Nucl. Mater. **463**, 769 (2015).

[16] A. M. Dimits, I. Joseph, and M. V. Umansky, Phys. Plasmas **21**, 055907 (2014).

[17] J.-Y. Ji and E. D. Held, Phys. Plasmas **15**, 102101 (2008).

[18] J.-Y. Ji, E. D. Held, and H. Jhang, Phys. Plasmas **20**, 082121 (2013).

[19] I. Joseph and A. M. Dimits, Contrib. Plasma Phys. **56**, 504 (2016).